J Biomol NMR (2007) 39:291–301
DOI 10.1007/s10858-007-9195-1

ARTICLE

Spatially encoded strategies in the execution of biomolecular-oriented 3D NMR experiments

Mor Mishkovsky · Maayan Gal · Lucio Frydman

Received: 19 July 2007 / Accepted: 5 September 2007 / Published online: 17 October 2007
© Springer Science+Business Media B.V. 2007

Abstract Three-dimensional nuclear magnetic resonance (3D NMR) provides one of the foremost analytical tools available for the elucidation of biomolecular structure, function and dynamics. Executing a 3D NMR experiment generally involves scanning a series of time-domain signals $S(t_3)$, as a function of two time variables (t_1, t_2) which need to undergo parametric incrementations throughout independent experiments. Recent years have witnessed extensive efforts towards the acceleration of this kind of experiments. Among the different approaches that have been proposed counts an "ultrafast" scheme, which distinguishes itself from other propositions by enabling—at least in principle—the acquisition of the complete multidimensional NMR data set within a single transient. 2D protein NMR implementations of this single-scan method have been demonstrated, yet its potential for 3D acquisitions has only been exemplified on model organic compounds. This publication discusses a number of strategies that could make these spatial encoding protocols compatible with 3D biomolecular NMR applications. These include a merging of 2D ultrafast NMR principles with temporal 2D encoding schemes, which can yield 3D HNCO spectra from peptides and proteins within $\approx$100 s timescales. New processing issues that facilitate the collection of 3D NMR spectra by relying fully on spatial encoding principles are also assessed, and shown capable of delivering HNCO spectra within 1 s timescales. Limitations and prospects of these various schemes are briefly addressed.

M. Mishkovsky · M. Gal · L. Frydman (✉)
Department of Chemical Physics, Weizmann Institute of Science, Rehovot 76100, Israel
e-mail: lucio.frydman@weizmann.ac.il

Keywords Multidimensional NMR · Fast acquisition methods · Spatial encoding · Ultrafast 3D NMR · HNCO NMR

Introduction

Nuclear magnetic resonance (NMR) spectroscopy plays a central role in Biology and Chemistry, as a unique analytical tool for the elucidation of biomolecular structure and dynamics (Becker 2000; Cavanagh et al. 1996). One-dimensional (1D) NMR experiments measure the resonance frequency of the spins, directly reflecting with a peak or multiplet the environment surrounding a particular atomic site. With increasing molecular weight, however, 1D methods begin lacking in the resolution that is needed for discerning each inequivalent nuclear position. This difficulty can be overcome through the use of multidimensional (≥2D) NMR spectroscopy (Jeener 1971; Aue et al. 1976; Ernst et al. 1987). Such methodology introduces additional frequency axes that spread out the information being sought into higher dimensions, thereby providing enough "space" to resolve the different peaks being sought. One of the few penalties that come associated with the many benefits brought about by increasing NMR's dimensionality, lies in the lengthier times that may be needed for completing the data acquisition process—times which may eventually become constrained by sampling rather than by sensitivity considerations. This is in part a consequence of the manner by which data are collected in multidimensional NMR experiments (Jeener 1971; Aue et al. 1976; Ernst et al. 1987): the signals associated to one of the spectral dimensions, the so-called direct domain, are physically monitored over a few hundreds of milliseconds in the usual pulsed NMR fashion

(Ernst and Anderson 1966). But the spins' evolution along the remaining dimensions gets monitored indirectly, using a discrete incrementation of associated time parameters throughout the pulse sequence. Collecting an a *n*-dimensional NMR spectrum will thus require setting tens, hundreds or thousands of different time delay combinations, set to sample all the different time axes while fulfilling the demands imposed by the data-processing protocol. As each of the several points required to characterize any of the indirect time-domains is associated with an independent signal acquisition, the overall experimental duration eventually increases exponentially with the number of involved dimensions.

In view of this feature, and stimulated in part by the increasingly important roles played by the routine acquisition of higher-dimensional NMR experiments and by the increased sensitivities characterizing modern spectrometers, recent years have witnessed extensive efforts geared at accelerating the acquisition of this kind of data (Kupce and Freeman 2003; Atreya and Szyperski 2005). Included among these efforts are Hadamard techniques compressing the acquisition by exploiting prior knowledge (Kupce and Freeman 2003; Kupce et al. 2003), projection-reconstruction and other "accordioned" sampling techniques achieving similar savings by incrementing various time parameters simultaneously (Ding and Gronenborn 2002; Kim and Szyperski 2003; Kupce and Freeman 2003; Hiller et al. 2005), relaxation-enhanced techniques that while using classical Fourier transform (FT) nD NMR schemes dramatically decrease the overall acquisition times by minimizing the interscan delay (Pervushin et al. 2002; Schanda and Brutscher 2005; Schanda et al. 2006), and non-FT based techniques that, based on a sparse sampling of the various time-domains, are no longer bound by the exacting demands of classic Nyquist criteria (Hoch and Stern 1996; Mandelshtam 2001; Luan et al. 2005; Brüschweiler and Zhang 2004).

Included among these emerging new methods are the so-called "ultrafast" NMR schemes (Frydman et al. 2002; 2003; Shrot and Frydman 2003), characterized by a capability to complete the full encoding demanded by nD FT acquisitions—at least in principle—within a single NMR scan. The essence of these methods as applied to the acquisition of 2D and 3D NMR spectra in liquid-state samples, is depicted in Fig. 1. At their core lies the idea of partitioning the sample into a series of independent subensembles, each of them encoding the kind of spin evolution that would have previously been associated with a particular indirect time-domain value. This partitioning can be achieved by applying continuously swept or frequency-stepped radiofrequency (RF) pulses, in combination with suitably echoed magnetic field gradients spreading out the spins' resonance frequencies along a particular direction r_i. Such combination allows one to imprint gradient-derived effects onto the spins' overall evolution; only internal evolution phases encoding the shift or coupling Ω parameters being sought, thus accrue at the conclusion of these procedures. When considered within the framework of Bloch's space (Fig. 1, lower panels) these pattern represent shift-induced windings of the spin coherences along the r_i encoding coordinate; such windings will in general be characterized by a

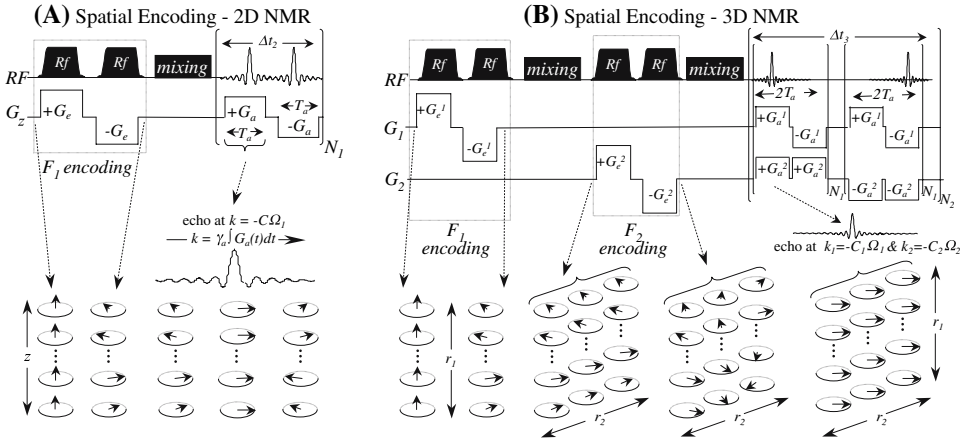

Fig. 1 Principles involved in the spatial encoding of 2D and 3D NMR data within a single-scan. RF blocks indicate frequency-chirped pulses which, when coupled to suitable magnetic field gradients G_e, achieve a sequential excitation of spins along the direction of the gradient. As these are applied in an alternating fashion no phase related to the spatial position of spins is retained, resulting in shift-driven helical windings along the gradient's direction (bottom). Following conventional, homogenous mixing sequences, data are collected while in the presence of oscillating acquisition gradients $\pm G_a$, capable of repetitively unwinding and winding the shift-induced spiral of spin-packets encoded during the excitation. The sharp echoes that are then generated unveil an array of indirect-domain spectra, modulated in the direct domain by final evolution frequencies accessible via FT

destructive interference among its constituent spin-packets, that will be preserved throughout the various coherent mixing processes involved in the nD NMR pulse sequence. At an acquisition stage, this spatially encoded information can then be extracted by applying suitable r_i-dependent gradients acting in combination with the data sampling. Such gradients will unwind the various helices that were subtended by the individual chemical sites, leading to observable echoes arising from constructive interference phenomena among spins positioned throughout the sample. Since the timing of such echoes will depend on the strengths of the Ω_i internal interactions being sought, this allows one to map all the indirect-domain spectra by monitoring the positions of the resulting echo "peaks", as described by the values taken by the wavenumbers $k_i = \gamma_i \int G_a^i(t)dt$ representing the action of the various unwinding gradients. Moreover, as such unwinding processes can be immediately reversed and repeated multiple times by alternating the signs of the various acquisition gradients, the direct-domain frequencies of the spins that are active during the final detection period can also be defined from the time modulation exhibited by such echoes. Subjecting the echo signals obtained during such a cyclic train of oscillating gradients to a suitable rearrangement and to a final 1D FT process along the direct domain thereby leads to the desired nD NMR spectrum—within a single scan.

This gradient-based approach to single-scan nD NMR has shown promising applications within the context of 2D protein spectroscopy (Shapira et al 2004; Gal et al. 2006, 2007), in the sense of being able to deliver a variety of homo- and hetero-nuclear 2D correlation spectra for biomolecules in the 1–3 mM concentration range, within second and sub-second timescales. In the present paper we focus on the prospects that these accelerated acquisition schemes could have towards the collection of 3D NMR data. Simple single-scan 3D and 4D NMR acquisitions have in fact been previously presented at proof-of-principle levels, based on demonstrations using highly concentrated (≥100 mM) organic samples (Frydman et al. 2003; Shrot and Frydman 2003). To explore the potential of such ultrafast-based methods within biomolecular 3D NMR scenarios, special attention is here placed on how to improve sensitivity while not unduly taxing the overall acquisition time. Alternatives explored include merging ultrafast 2D NMR and fast-repetition temporal encoding principles into a common acquisition mode, capable of delivering 3D HNCO protein NMR spectra within a minutes-timescale. We also discuss the prospects of using new data acquisition and processing formats in experiments relying on fully spatially encoded 3D NMR, for improving the performance of the original protocol and thus yield further reductions on the overall acquisition times.

Materials and methods

The results described in this work were measured either on a Bruker Avance® 800 MHz NMR spectrometer, or on a Varian Inova® 500 MHz machine. Both of these spectrometers incorporated multiple-resonance (HCN) inverse probes of similar sample sizes (≈18 mm long × 4.9 mm dia) as well as triple-axes gradients with similar maximal performances (≈60 G/cm along the longitudinal and ≈30 G/cm along the transverse axes). The typical gradient switching times were also similar on both systems (≈10 μs); sensitivity-wise, the 800 MHz spectrometer performed ca. twice as good as the 500 MHz machine on a per-scan basis. A central ingredient of all assayed pulse sequences was the application of pairs of frequency-swept pulses, acting in coordination with excitation gradients $\pm G_e$ so as to spatially encode the internal interactions of interest. These frequency-chirped pulses extended over bandwidths $\pm\gamma_i G_e^i L_i/2$ for each independent i-dimension; they were programmed as smoothed-amplitude and phase tables using the Pbox® and Stdisp® programming tools included in the Varian and Bruker spectrometers, and their overall offsets were suitably shifted so as to conform to the non-quadrature detection characterizing the indirect-domain spectral detection of spatially-encoded NMR (Fig. 1). All data were processed off-line using a variety of custom-written Matlab® 7 software packages. The analyzed samples included a custom-made, uniformly (^{13}C,^{15}N)-enriched tripeptide composed of Leucine-Alanine-Phenylalanine (LAF) dissolved at a 2.0 mM concentration in an HDO/d_6–DMSO solution, and an aqueous (90% H_2O) solution of U-^{15}N/^{13}C Ubiquitin (Histidine-tagged form, Asla Ltd., Latvia) dissolved at a 2.0 mM concentration in a 50 mM sodium phosphate buffer.

Results

Incorporating spatially encoded 2D schemes into 3D NMR sequences

As mentioned, single-scan 2D NMR spectra can be successfully recorded on small proteins when concentrations are in the low-mM range. Additional sensitivity losses, such as those that will arise upon incorporating a second mixing period in the sequence or upon further reducing the sample's concentration, could be accounted for by a concomitant increase in the number of averaged scans. Such signal averaging would take place in a natural fashion upon extending the dimensionality of a 2D experiment onto a third dimension, with the conventional sampling of an additional indirect-domain raising sensitivity according to the multiplex advantage (Ernst et al. 1987). In other words, one could offset the losses associated to ultrafast 2D NMR

by adding onto such sequence a conventional temporal encoding block. In the resulting 'hybrid' 3D sequence only one of the indirect domains would then become spatially encoded, whereas the other would be monitored using a conventional temporal incrementation routine. The experimental time required for acquiring 3D NMR information using such combined spatial/temporal encoding approach would still be substantially reduced in comparison to conventional counterparts. We have recently described the conditions that have to be met if such approach is to be used in combination with projection-reconstruction methods (Mishkovsky et al. 2007); we focus here on the design of a 'hybrid' ultrafast-conventional pulse sequence geared at 3D HNCO NMR acquisitions. This experiment can correlate ^{1}H and ^{15}N peaks of a given amide group with the carbonyl ^{13}C peak belonging to the previous residue, thereby mapping a protein according to its amide backbone (Ikura et al. 1990; Sattler et al. 1999). Out of the various alternatives that could be considered for incorporating into a 3D HNCO sequence joint spatial and temporal encodings, the scheme shown in Fig. 2A was chosen. In it, the chemical shifts of ^{1}H-enhanced ^{15}N sites are spatially encoded within a single scan along the sample's z axis, while ^{13}C interactions are monitored in a multi-scan fashion using a conventional t_2 incrementation. Both of these schemes were incorporated as amplitude-modulated real-time HSQC encoding periods, with chirped $\pi/2$ pulses triggering the excitation and storage of spatially-encoded $2H_zN_x$ terms during F1 (Shrot et al. 2004), hard $\pi/2$ pulses converting these terms in and out of $4H_zN_zC_x$ three-spin coherences during t_2, and conventional INEPT transfers (Morris and Freeman 1979) in-between the various periods. Full heteronuclear decoupling was achieved for all domains by the incorporation of π refocusing pulses; along the spatially encoded and the direct domains, this proofed more practical than continuous decoupling sequences owing to the presence of gradient effects during the course of these spin evolutions. The resulting 3D experiment was tested first on a 2 mM solution of the U-^{15}N/^{13}C labeled tripeptide LAF, to confirm whether the multiplex advantage along t_2 can compensate for the ultrafast- and mixing-derived losses. It could be concluded (Fig. 2C) that ca. 1.5 min total acquisition times sufficed to obtain 3D NMR spectra from this small molecule, on a 500 MHz spectrometer equipped with a conventional room-temperature probe.

The kind of hybrid spatial/temporal 3D sequences just presented could be accelerated further when dealing with protein systems, if one were to rely on relaxtion-enhanced schemes permitting a rapid scanning of the incremented temporal parameter (Pervushin et al. 2002). As recently demonstrated (Schanda and Brutscher 2005; Schanda et al. 2006) a substantial decrease in the experimental acquisition times can be achieved using selective spin excitation for

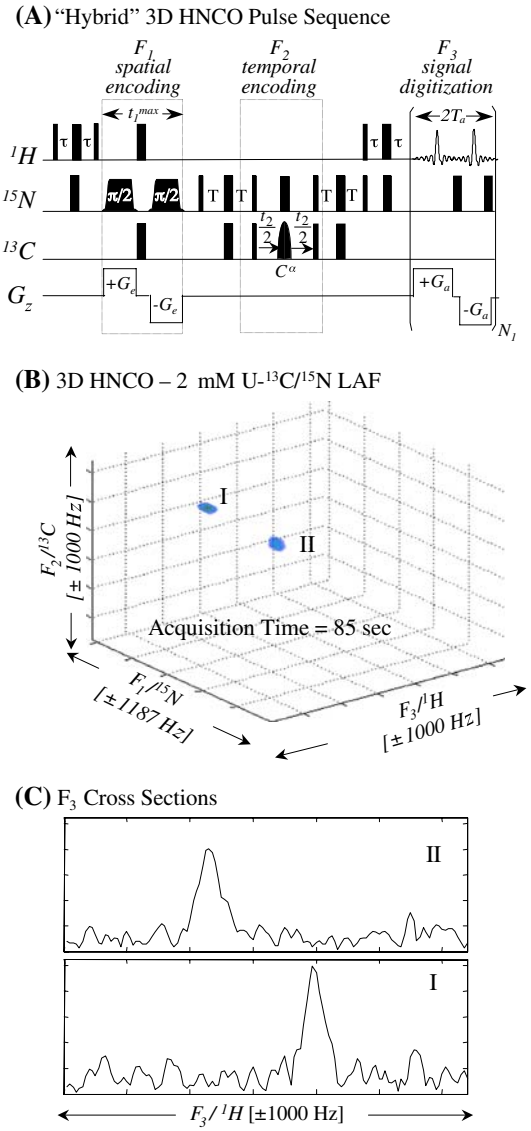

Fig. 2 (**A**) Pulse sequence assayed for the accelerated acquisition of 3D HNCO spectra, with the ^{15}N dimension spatially encoded along the z axis and ^{13}C interactions monitored using a conventional temporal encoding. Data in the resulting ultrafast 2D planes need then to be suitably rearranged (Frydman et al. 2003) and FT'd along the t_2, t_3 temporal dimensions. Narrow and wide bars denote non-selective $\pi/2$ and π pulses respectively; also indicated are the frequency-swept spatial-encoding pulses ($\pi/2$ labels), as well as a selective C^{α} π-pulse applied during t_2 for decoupling purposes. All ^{13}C pulses affected the CO resonance region except for the C^{α}-specific π inversion (shaped pulse). (**B**) Experimental 3D spectrum collected on a 2 mM LAF peptide in d_6-DMSO at 500 MHz, in a total acquisition time of 85 s. Additional experimental parameters included t_1^{max} = 10 ms, T_a = 500 μs, G_e = 40 G/cm, G_a = 6.2 G/cm, N_1 = 32, heteronuclear coherence transfer delays τ = 2.5 ms, T = 16 ms. For the ^{13}C dimension Δt_2 = 500 μs and 16 time increments were used; overall, 64 scans with a recycle delay of 1.3 s were accumulated. (**C**) Cross-sections arising from the indicated peaks in the 3D HNCO spectrum

experiments which, like ^{1}H-^{15}N HSQC or ^{1}H-^{15}N-^{13}CO, focus only on a minority of the protons present in the molecule. Such selectivity allows for longitudinal

Fig. 3 3D HNCO results stemming from a relaxation-optimized hybrid approach akin to that in Fig. 2A, but with certain ^{1}H RF manipulations made band-selective. These pulses are denoted by shaped ^{1}H profiles, with open and filled shapes corresponding to $\pi/2$ and π flip angles respectively; they were designed with durations of 1.5 ms based on the SLR algorithm (Pauly et al. 1991) so as to be 4 ppm wide, and adjusted to deliver a null excitation at the water chemical shift position by centering them at 8 ppm. Selective Sinc-shaped Carbon pulses were used as well, with CO/C$^{\alpha}$ pulses exhibiting null excitation on the C$^{\alpha}$/CO regions respectively. (**B**, **C**) Full 3D HNCO spectra recorded on a 2 mM U-^{15}N/^{13}C Ubiquitin sample in 90% H_2O. The spectrum shown in (**B**) was acquired in 16 min using 1024 overall scans with a 0.5 s recycle delay, while the spectrum in (**C**) one was acquired using 256 scans and 0.35 s recycle. Both spectra were collected on a 500 MHz spectrometer equipped with a conventional triple-axis HCN probehead, and their final matrix sizes were $128 \times 2048 \times 32$ points along the ^{1}H, ^{15}N and ^{13}C dimensions. Other experimental parameters included heteronuclear coherence transfer delays $\tau = 1.2$ ms (empirically optimized in conjunction with the SLR pulses) and T = 16 ms, $t_1^{max} = 10$ ms, $G_e = 40$ G/cm, $G_a = 1.76$ G/cm, $T_a = 1.25$ ms, $N_1 = 32$, 16 t_2 increments, $\Delta t_2 = 256$ µs. Four scans were interleaved for each carbon plane (Matsui et al. 1985; Vold and Vold 1986) in order to minimize the direct-domain filter bandwidth down to a value of 6 kHz. Further views of these data are given in Fig. 4

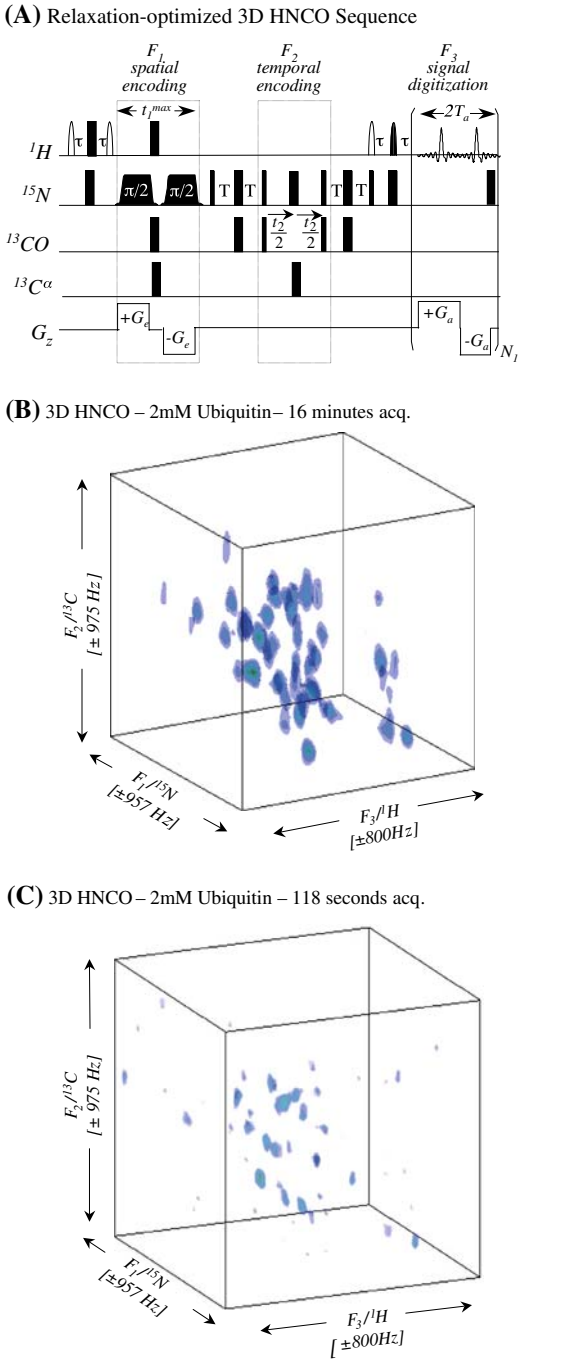

cross-relaxation enhancement to occur between the majority of non-excited spins and the excited ones, leading to a significant shortening of the recycling delays that are necessary before repeating the multiple scans involved in the experiment. An example of how such an advantage can be brought to bear in 3D sequences of the kind being here considered is presented in Fig. 3, together with experimental results arising from the sequence's execution on a U-^{15}N/^{13}C Ubiquitin sample. Like the counterpart introduced in Fig. 2 this sequence is also based on a real-time amplitude-modulated spatial encoding of the ^{15}N, followed by a conventional ^{13}C parametric incrementation. Amide protons, however, were now selectively excited with narrowband $\pi/2$ ^{1}H RF pulses designed using the SLR algorithm (Pauly et al. 1991), leading to the longitudinal relaxation enhancement effects that were sought. Optimal signal-to-noise ratios (SNRs) were found when retaining a pair of conventional ^{1}H π pulses (which overall restore the non-amide and the water protons back to their z-state equilibrium within a short period), rather than by using selective ^{1}H pulses throughout the pulse sequence. To further increase the experimental SNR the acquisition gradients were reduced by incorporating an adjustable delay prior to the beginning of the acquisition, which allowed for the co-addition of four interleaved data scans per indirect-domain t_2 value (Frydman et al. 2003; Matsui et al. 1985; Vold and Vold 1986). Full 3D HNCO NMR spectra could then be collected on a 2 mM Ubiquitin solution at timescales that, on a conventional 500 MHz spectrometer, reached down to just a few minutes. Selected 2D N-H planes extracted out of these full 3D HNCO spectra for different signal averaging times, are illustrated for clarity in Fig. 4.

Full spatially encoded ultrafast 3D NMR incorporating interlaced processing

As discussed in Fig. 1, incorporating multiple linearly independent gradient geometries could enable one to collect the kind of 3D spectra just discussed within much

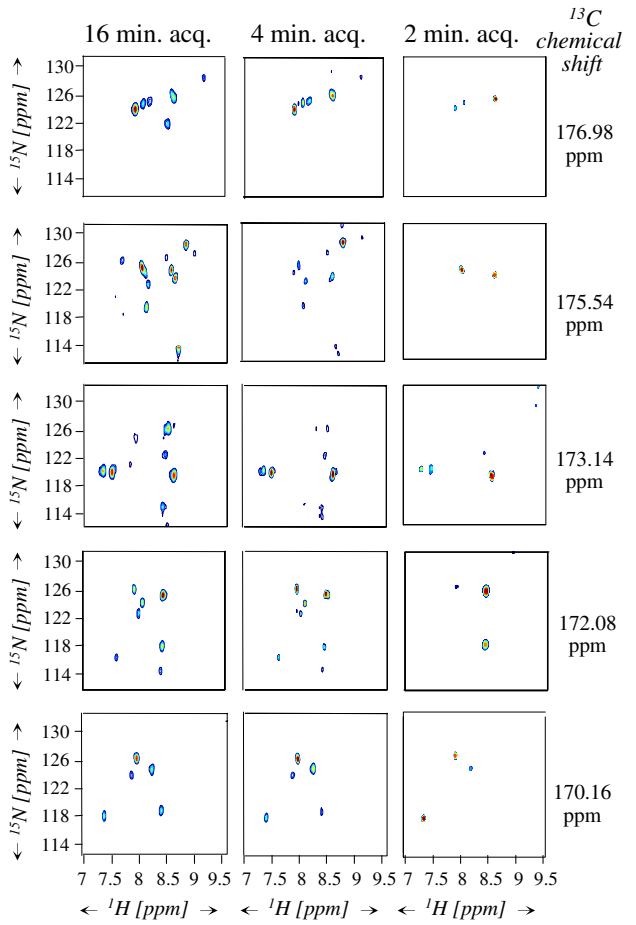

Fig. 4 Representative N-H planes taken from different 3D HNCO spectra collected using the parameters shown in Fig. 3, and the indicated total acquisition times. Denoted on the right is the center frequency of the specified ^{13}C plane. Contours were chosen above the noise level, so as to illustrate the peaks observable as a function of decreasing signal averaging times

shorter time scales. On considering the adoption of such routes it follows that frequencies along the two indirect domains would have to be spatially encoded, and the t_3-domain monitored in the usual direct fashion. While this could indeed lead to a dramatic reduction in the overall acquisition time required for the completion of 3D NMR experiments, such gain would not come for free. Ultrafast NMR spectroscopy suffers form a decrease in sensitivity because of its concomitant sampling of multiple domains. Extending the echo-planar sampling involved in 2D spectroscopy to an echo-volume 3D sampling would require opening even further the receiving filter bandwidth, which will in general be given by $\gamma_a\sqrt{\sum_i G_{a,i}^2 L_i^2}$ being the sample's length along the r_i-dimension (Shrot and Frydman 2003). This increase in receiver bandwidth over what would be a conventional $\sim(\Delta t_3)^{-1}$ value, may result in a substantial per-scan SNR penalty. In addition to these acquisition-related losses, sensitivity may be further compromised by the approach used to process the ultrafast NMR data. Indeed ultrafast acquisitions are characterized by gradient-driven analog FTs of the evolutions encoded along the spatial domains, coupled to a numerical 1D transformation against the direct domain for reconstructing the final spectrum. Data collected under the action of alternating positive and negative gradients, however, cannot be processed along the direct domain using a single fast FT of the full set, since the resulting data points do not appear spaced within a regular Cartesian grid. To carry out such a Fourier analysis while still relying on the fast FT algorithm the collected data need to be separated into two independent subsets, associated with the positive- and the negative-gradient acquisition periods. Each of these will then exhibit equally spaced points along the direct time-domain (Fig. 5A); but lead in turn to a certain sensitivity sacrifice, as well as to progressively smaller spectral bandwidths. For instance in the 2D case only half of the data points would be used within each FT(t_2) processing. In the ultrafast 3D case the situation is even more onerous, with only a quarter of the acquired points being ready for fast FT processing (Fig. 5B). As a consequence the effective dwell time along the direct domain becomes progressively longer within the individually sub-sets, making the covering of specified direct- and indirect-domain spectral widths more demanding in terms of the acquisition gradients required.

On the other hand, if it were possible to combine both positive- and negative-gradient data subsets into a single FT operation, the increased number of data points being processed coupled to the decrease in the effective dwell time that would result should ease up the gradient strength requirements, thereby leading to a sensitivity improvement. A simple procedure that can deal with this kind of data distribution is the interlaced FT (Bracewell 1978). This reconstruction scheme, which has been demonstrated for a number of MRI settings (Sekihara and Kohno 1987; Metzger and Hu 1997), can jointly process two arrays of data points whose individual spacing is given by identical increments Δt but which are shifted from one another by an interval $\tau \neq \Delta t/2$—and still lead to a common spectral bandwidth of $2/\Delta t$. As can be appreciated from Fig. 5 this is exactly the kind of scenario arising along the temporal domain in ultrafast 2D NMR for every value of k except for the special rows located at $k = 0$ and $\pm k_{max}$, where data points appear *a priori* equally spaced by the sampling. For all other non-uniform spacing cases, the interlaced FT can be used to unravel peaks over a frequency bandwidth of $2/\Delta t$, starting from the fast FT of the two non-coincident time-domain data sets sampled at $1/\Delta t$ dwell rates. This is achieved by a suitable linear combination of the data's FTs, which allows one to distinguish peaks falling within the $-1/(2\Delta t) \leq \nu \leq 1/(2\Delta t)$ interval, from those resonating

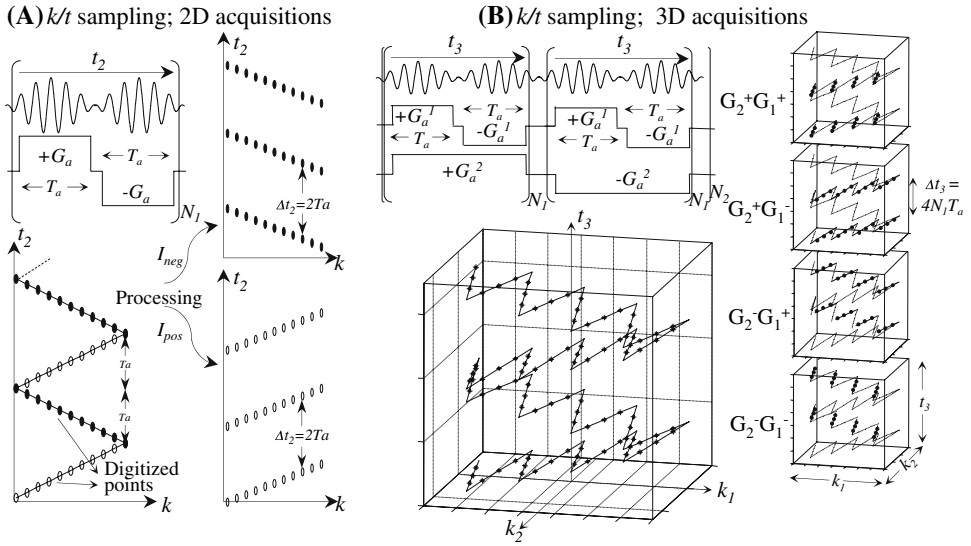

Fig. 5 Complications arising upon scanning mixed *k*(frequency)/*t*(direct-domain) acquisition spaces in ultrafast nD NMR. (**A**) 2D case, where signals are digitized continuously (open and closed dots) while under the action of positive and negative acquisition gradients. Data points stemming from such a scheme are not arrayed within a regular grid ready to be fast FTd, unless processed into the two indicated bidimensional data sets I_{pos}, I_{neg} (right). (**B**) (k_1,k_2,t_3) acquisition-space arising in a 3D case. In analogy to the single scan 2D processing procedure, fast FT of points acquired in such fashion require a preliminary discrimination according to their $\pm G_1$, $\pm G_2$ values (right, dotted traces). The interlaced FT procedure described in the text combines all these subsets into a single, common processing procedure

in the outer $|1/(2\Delta t)| \le \nu \le |1/\Delta t|$ ranges. For the 2D ultrafast NMR case this procedure would involve computing the {FT[$I_{pos}(k,t)$], FT[$I_{neg}(k,t)$]} spectra arising from the separate processing of positive- and negative-gradient arrays, and using them to calculate two new spectral distribution functions:

$$G(k,\nu) = -\frac{\exp[-i\cdot sg(\nu)\pi\tau/\Delta t]}{1-\exp[-i\cdot sg(\nu)\pi\tau/\Delta t]}FT\left[I_{pos}(k,t)\right] + \frac{\exp(-i\cdot 2\pi\tau\nu)}{1-\exp[-i\cdot sg(\nu)\pi\tau/\Delta t]}FT\left[I_{neg}(k,t)\right]$$

$$H(k,\nu) = \frac{1}{1-\exp[-i\cdot sg(\nu)\pi\tau/\Delta t]}FT\left[I_{pos}(k,t)\right] + \frac{\exp(-i\cdot 2\pi\tau\nu)}{1-\exp[-i\cdot sg(\nu)\pi\tau/\Delta t]}FT\left[I_{neg}(k,t)\right].$$

These functions enable one in turn to characterize the 2D $I(k,\nu)$ spectrum over a full $2/\Delta t$ direct-domain spectral range, according to the reconstruction recipe.

$$I(k,\nu) = \begin{cases} H(k,\nu+1/\Delta t), & -1/\Delta t \le \nu \le -1/2\Delta t \\ G(k,\nu), & -1/2\Delta t \le \nu \le +1/2\Delta t \\ H(k,\nu-1/\Delta t), & +1/2\Delta t \le \nu \le +1/\Delta t \end{cases}$$

Notice that while these manipulations manage to successfully multiplex all the digitized data points, they demand both an *a priori* knowledge of the time τ separating both data sets for every k value, as well as equal intensities of I_{pos} and I_{neg}. Minor miss-timings in the former or imbalances in the latter may originate residuals positioned $\pm 1/(2\Delta t)$ from the genuine peaks, visible sometimes in the spectra (Mishkovsky and Frydman 2005).

The applicability of this processing scheme and its ensuing improvements, were recently demonstrated within the context of single-scan 2D NMR (Mishkovsky and Frydman 2005). We focus here on the even higher rewards that could result from implementing the interlaced FT processing along the t_3 domain of an ultrafast 3D acquisition. Consideration of how points are distributed within the digitized (k_1,k_2,t_3)-space (Fig. 5B) leads to the realization that interlacing will still take place in these experiments in a pair-wise fashion, between subspectra of opposite (k_1,k_2) polarities. In other words two linear combinations of the kind described above will have to be now computed: one for $I_{pos,pos}(k_1,k_2,t_3)$ and $I_{neg,neg}(k_1,k_2,t_3)$; the other between $I_{pos,neg}(k_1,k_2,t_3)$ and $I_{neg,pos}(k_1,k_2,t_3)$. For a given k_1 or k_2 point, the grid subtended in the corresponding orthogonal data sub-set ((k_1,t_3) or (k_2,t_3)) will display the same "zig-zagging" trajectory as that encountered in 2D acquisitions. The equations presented before will consequently still be suitable for dealing with these 3D data and lead to a $\sqrt{2}$ sensitivity enhancement reflecting the increase in the number of data points that were jointly co-processed. Moreover, once all data have been cast in a common (k_1/ν_1,k_2/ν_2,ν_3) space, it becomes possible to

merge the two interlaced sets that were independently FT'd, doubling the effective spectral resolution along both indirect-domain axes. Notice that this is accomplished while simultaneously reducing the intensities required from G_a^1/G_a^2 to cover a pre-defined spectral range, thereby reducing the expected receiver bandwidth as well. This increases SNR by another $\sqrt{2}$ factor in comparison to the fast FT of a single data set.

A number of tests were carried out in order to examine the arguments just summarized. The first one focused on the method's actual ability to increase the net spectral bandwidth that could be faithfully covered along the direct domain. The performance afforded by the procedure in this respect can be appreciated from Fig. 6, which compares fast- and interlaced-FT results arising in a simple, mixing-less single-scan 3D NMR experiment on a model compound. In order to test the consequences of the sensitivity enhancement and larger bandwidth afforded by the interlaced FT, a 3D HNCO acquisition based on this protocol was repeated on the 2 mM LAF tripeptide solution. By contrast to the spatial encoding tests described so far, which were based on a real-time encoding of the indirect domains, this heteronuclear acquisition was based on a constant-time encoding modality based on adiabatic π encoding pulses (Pelupessy 2003). Measuring this kind of heteronuclear correlation spectra would have been challenging using the ultrafast data processing mode employed in Ref. (Shrot and Frydman 2003), both because of sensitivity considerations as well as due to difficulties in accommodating the necessary spectral bandwidths utilizing

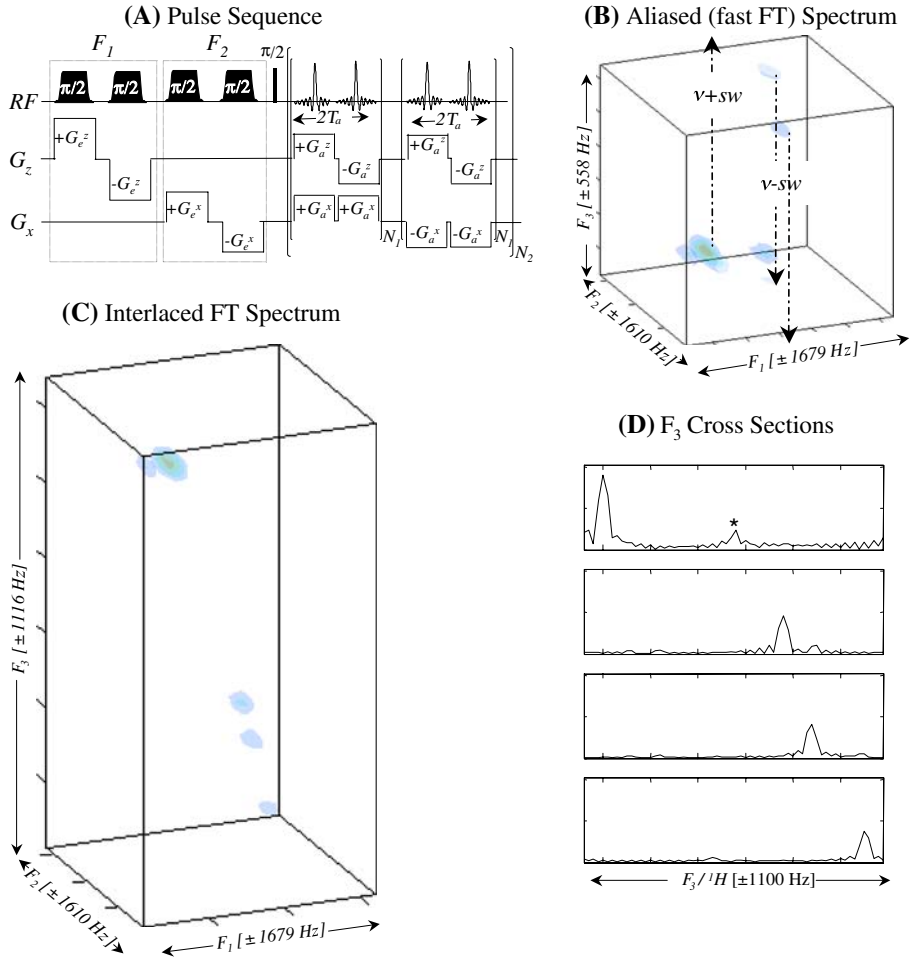

Fig. 6 Single scan ^{1}H ultrafast 3D NMR spectra of n-butylchloride/$CDCl_3$ measured at 800 MHz on a Bruker spectrometer using QXI probe. (**A**) Basic homonuclear mixing-less pulse sequence tested in the experiment, with each indirect domain spatially encoded using a continuous amplitude modulation scheme. Whereas a full spectral bandwidth coverage was not possible upon using the conventional fast FT processing of these data (**B**), this becomes possible upon using an interlaced FT processing (**C**). Dashed arrows in (**B**) show the ways by which peak positions should unfold for obtaining the actual chemical shifts; the asterisk in (**D**) corresponds to a minor $SW_3/2$ artifact associated with the data interlacing. Parameters associated with the experiment included t_1^{max} = 5 ms, G_e^z = 6.34 G/cm, t_2^{max} = 4 ms, G_e^z = 6.00 G/cm. T_a = 48 μs, G_a^x = 19.71 G/cm, G_a^z = 45.65 G/cm, a filter bandwidth of 352 kHz, N_1 = 4, N_2 = 16, and a single scan. The minor peak indicated by an asterisk in (**D**) illustrates an interlaced FT artifact of peaks appearing close to the edges of *k* space (Sekihara and Kohno 1987)

the commonly available gradient strengths. The application of the interlaced FT processing enables a simultaneous alleviation of both considerations, leading to the successful acquisition of a 3D HNCO spectrum with meaningful spectral parameters on a 2 mM sample within just a couple of scans—as opposed to the minutes timescales that would normally be associated with this kind of experiments (Fig. 7).

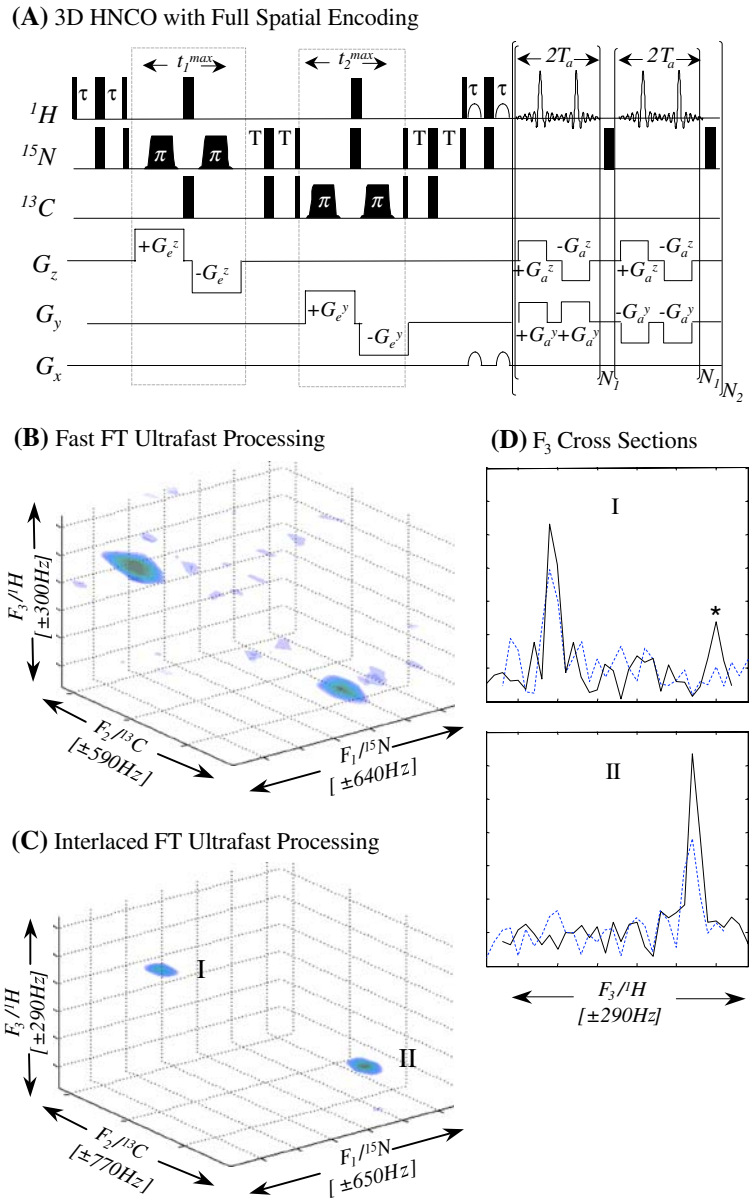

Fig. 7 3D ultrafast HNCO tests on U-^{15}N/^{13}C LAF in d_6-DMSO/H_2O. (**A**) Pulse sequence involving spatial encoding of the ^{15}N (F_1) along the z axis, and of the ^{13}C (F_2) along the y axis. Both spatial encodings were carried out using a continuous, constant-time scheme (Pelupessy 2003); residual solvent was eliminated via a Watergate protocol (Piotto et al. 1992) prior to the acquisition using a homospoil gradient along the x axis. (**B**, **C**) Fast FT and interlaced FT processing data set collected in only 2 scans (for the sake of phase cycling away artifacts) on an 800 MHz spectrometer using a QXI probe. Both spectra are presented at the same threshold levels and were collected with identical encoding parameters: G_e^z = 31.7 G/cm, t_1^{max}= 9.72 ms (encoding of ^{15}N along z axis), t_2^{max} = 3.87 ms, G_a^y = 18.56 G/cm (encoding of ^{13}C along y axis), and τ, T delays set at 2.5 and 15 ms for optimized transfers. Acquisition parameters for the fast FT processing experiments were G_a^z = 25.36 G/cm, G_a^y= 2.86 G/cm, T_a = 64 µs and a 194.4 kHz filter bandwidth; for the interlaced FT processing these parameters were G_a^z = 15.85 G/cm, G_a^y = 2.29 G/cm, T_a = 104 µs, and a reduced receiver bandwidth of 120 kHz. Final matrix sizes were 34 × 12 × 16 and 54 × 12 × 16 in (**B**) and (**C**), respectively. (**D**) Compares traces arising from the fast and from the interlaced FT spectra (continuous black and dashed blue traces, respectively). Once again, the asterisk reflects a minor interlaced-derived artifact

Discussion and conclusions

The present study discussed a number of strategies that, by relying on spatial encoding protocols, enable one to shorten the acquisition times required for completing the collection of full 3D NMR data sets. The ability of spatial encoding to accelerate this kind of spectral acquisitions is put to a stringent test when analyzing biomolecules at low mM concentrations—particularly when envisioning their use for the detection of transient intermediates in dynamically changing systems. Still we believe that the results that were here presented are quite encouraging, as 3D HNCO acquisitions ranging from a few minutes and down to a few seconds were proven possible. Yet at the same time it is clear that a number of obstacles remain to be overcome before these sequences become routine—even within a research-oriented environment. The main one, of course, remains the issue of SNR. Based on the data presented in Paragraph 3.1, collected on a 500 MHz NMR spectrometer, we believe that hybrid acquisitions of this kind should become feasible at $\sim$1 mM concentrations and/or on $\sim$10 s timescales, if switched to a high-field (≥800 MHz) cryogenically-cooled platform. Even shorter acquisition times might be possible if switching the indirect-domain sampling to a projection-reconstruction kind of scheme (Mishkovsky et al. 2007); additional sensitivity improvements may originate from introducing proton decoupling during the heteronuclear $^{15}N \leftrightarrow {}^{13}C$ transfer periods, or by adding sensitivity-enhanced $^{15}N \rightarrow {}^{1}H$ transfer modules. These various possibilities are currently being tested. Harder to test are the options opened by cryogenically-cooled hardware on the fully spatially encoded experiments described in Paragraph 3.2, as all commercial platforms of this kind currently devoid of the multi-axial gradients needed to implement this kind of experiments. Perhaps this state of affairs will change; perhaps the advent of other developments in the field, such as nuclear hyperpolarization methods enabling the detection of unusually low sample concentrations, can enable further progress of nD ultrafast NMR protocols even using room temperature probes (Ardenkjaer-Larsen et al. 2003; Frydman and Blazina 2007). We trust to report on some of these opportunities in upcoming studies.

Acknowledgments We are grateful to Mr. Yoav Shrot for his computation of the SLR pulses, and to Dr. Paul Schanda (IBS, Grenoble) for useful discussions. This work was supported by the Israel Science Foundation (ISF 1206/05) and by the European Commission (EU-NMR contract No.026145), and made possible in part by the generosity of the Perlman Family foundation.

References

Ardenkjaer-Larsen JH, Fridlund B, Gram A, Hansson G, Hansson L, Lerche MH, Servin R, Thaning M, Golman K (2003) Increase in signal-to-noise ratio of >10,000 times in liquid-state NMR. Proc Natl Acad Sci USA 100:10158–10163

Atreya HS, Szyperski T (2005) Rapid NMR data collection. Methods Enzymol 394:78–108

Aue WP, Bartholdi E, Ernst RR (1976) Two-dimensional spectroscopy. Application to nuclear magnetic resonance. J Chem Phys 64:2229–2246

Becker B (2000) High resolution NMR. Academic Press, New York

Bracewell RN (1978) The Fourier transform and its application. McGraw-Hill, New York

Brüschweiler R, Zhang F (2004) Covariance nuclear magnetic resonance spectroscopy. J Chem Phys 120:5253–5260

Cavanagh J, Fairbrother WJ, Palmer AG, Skelton NJ (1996) Protein NMR spectroscopy: principles and practice. Academic Press, San Diego

Ding K, Gronenborn A (2002) Novel 2D triple resonance NMR experiments for sequential resonance assignments of proteins. J Magn Reson 156:262–268

Ernst RR, Anderson WA (1966) Application of Fourier transform spectroscopy to magnetic resonance. Rev Sci Instr 37:93–102

Ernst RR, Bodenhausen G, Wokaun A (1987) Principles of nuclear magnetic resonance in one and two dimensions. Clarendon, Oxford

Frydman L, Blazina D (2007) Ultrafast two-dimensional nuclear magnetic resonance spectroscopy of hyperpolarized solutions. Nat Phys 3:415–419

Frydman L, Scherf T, Lupulescu A (2002) The acquisition of multidimensional NMR spectra within a single scan. Proc Natl Acad Sci USA 99:15858–15862

Frydman L, Scherf T, Lupulescu A (2003) Principles and features of single-scan two-dimensional NMR spectroscopy. J Am Chem Soc 125:9204–9217

Gal M, Mishkovsky M, Frydman L (2006) Real time monitoring of chemical transformations by ultrafast 2D NMR spectroscopy. J Am Chem Soc 128:951– 956

Gal M, Schanda P, Brutscher B, Frydman L (2007) UltraSOFAST HMQC NMR and the repetitive acquisition of 2D protein spectra at Hz rates. J Am Chem Soc 129:1372–1377

Hiller S, Fiorito F, Wüthrich K (2005) Automated projection spectroscopy (APSY). Proc Natl Acad Sci USA 102:10876–10881

Hoch JC, Stern AS (1996) NMR data processing. Wiley-Liss, New York

Ikura M, Kay LE, Bax A (1990) A novel approach for sequential assignment of 1H, 13C, and 15N spectra of proteins: heteronuclear triple-resonance three-dimensional NMR spectroscopy. Application to calmodulin. Biochemistry 29:4659–4667

Jeener J (1971) Unpublished lecture in Ampere International Summer School II. Basko Polje, Yugoslavia

Kim S, Szyperski T (2003) GFT NMR, a new approach to rapidly obtain precise high dimensional NMR spectral information. J Am Chem Soc 125:1385–1393

Kupce E, Freeman R (2003) Reconstruction of the three-dimensional NMR spectrum of a protein from a set of plane projections. J Biomol NMR 7:383–387

Kupce E, Freeman R (2003) New methods for fast multidimensional NMR. J Biomol NMR 27:101–114

Kupce E, Freeman R (2003) Two-dimensional Hadamard spectroscopy. J Magn Reson 162:300–310

Kupce E, Nishida T, Freeman R (2003) Hadamard NMR spectroscopy. Progr Nucl Magn Reson Spectroscopy 42:95–122

Luan T, Orekhov VY, Gutmanas A, Billeter M (2005) Accuracy and robustness of three-way decomposition applied to NMR data. J Magn Reson 174:188–199

Mandelshtam VA (2001) FDM: the filter diagonalization method for data processing NMR experiments. Progr Nucl Magn Reson Spectroscopy 38:159–196

Matsui S, Sekhiara K, Kohno H (1985) High speed spatially-resolved NMR spectroscopy using phase-modulated spin-echo trains. Expansion of the spectral bandwidth by combined use of delayed spin-echo trains. J Magn Reson 64:167–171

Metzger G, Hu X (1997) Application of interlaced fourier transform to echo-planar spectroscopic imaging. J Magn Reson 125: 166–170

Mishkovsky M, Frydman L (2005) Interlaced Fourier transformation of ultrafast 2D NMR data. J Magn Reson 173:344–350

Mishkovsky M, Kupce E, Frydman L (2007) Ultrafast-based projection reconstruction 3D nuclear magnetic resonance spectroscopy. J Chem Phys 127:034507

Morris GA, Freeman R (1979) Enhancement of nuclear magnetic resonance signals by polarization transfer. J Am Chem Soc 101:760–762

Pauly J, Le Roux P, Nishimura D, Macovski A (1991) Parameter relations for the Shinnar-Le Roux selective excitation pulse design algorithm. NMR Imaging Trans Med Imag 10:53–65

Pelupessy P (2003) Adiabatic single-scan 2D NMR spectroscopy. J Am Chem Soc 125:12345–12350

Pervushin K, Voegeli B, Eletsky A (2002) Longitudinal H-1 relaxation optimization in TROSY NMR spectroscopy. J Am Chem Soc 124:12898–12902

Piotto H, Saudek V, Sklenar V (1992) Gradient-tailored excitation for single-quantum NMR spectroscopy of aqueous solutions. J Biomol NMR 2:661–665

Sattler M, Schleucher J, Griesinger C (1999) Heteronuclear multidimensional NMR experiments for the structure determination of proteins in solution emplying pulsed field gradients. Progr Nucl Magn Reson Spectroscopy 34:93–158

Schanda P, Brutscher B (2005) Very fast two-dimensional NMR spectroscopy for real-time investigation of dynamic events in proteins on the time scale of seconds. J Am Chem Soc 127:8014–8015

Schanda P, Van Melckebeke H, Brutscher B (2006) Speeding up three-dimensional protein NMR experiments to a few minutes. J Am Chem Soc, 128:9042–9043

Sekihara K, Kohno H (1987) New reconstruction technique for echo planar imaging to allow combined use of odd and even numbered echoes. Magn Reson Med 5:485–491

Shapira B, Lupulescu A, Shrot Y, Frydman L (2004) Line shape considerations in ultrafast 2D NMR. J Magn Reson 166:152–166

Shrot Y, Frydman L (2003) Single-scan NMR spectroscopy at arbitrary dimensions. J Am Chem Soc 125:11385–11396

Shrot Y, Shapira B, Frydman L (2004) Ultrafast 2D NMR spectroscopy using a continuous spatial encoding of the spin interactions. J Magn Reson 171:162–169

Vold RR, Vold RL (1986) Nyquist frequency extension by interleaved data acquisition. J Magn Reson 70:144–148